NANO LETTERS

Letter

pubs.acs.org/NanoLett

Photonic Multitasking Interleaved Si Nanoantenna Phased Array

Dianmin Lin,[†,‡] Aaron L. Holsteen,[†] Elhanan Maguid,[§] Gordon Wetzstein,[‡] Pieter G. Kik,[∥] Erez Hasman,[§] and Mark L. Brongersma*[,†]

[†]Geballe Laboratory for Advanced Materials, Stanford University, Stanford, California 94305, United States

[‡]Department of Electrical Engineering, Stanford University, Stanford, California 94305, United States

[§]Micro and Nanooptics Laboratory, Faculty of Mechanical Engineering and Russell Berrie Nanotechnology Institute, Technion−Israel Institute of Technology, Haifa 32000, Israel

[∥]CREOL, The College of Optics and Photonics, University of Central Florida, Orlando, Florida 32816, United States

Supporting Information

ABSTRACT: Metasurfaces provide unprecedented control over light propagation by imparting local, space-variant phase changes on an incident electromagnetic wave. They can improve the performance of conventional optical elements and facilitate the creation of optical components with new functionalities and form factors. Here, we build on knowledge from shared aperture phased array antennas and Si-based gradient metasurfaces to realize various multifunctional metasurfaces capable of achieving multiple distinct functions within a single surface region. As a key point, we demonstrate that interleaving multiple optical elements can be accomplished without reducing the aperture of each subelement. Multifunctional optical elements constructed from Si-based gradient metasurface are realized, including axial and lateral multifocus geometric phase metasurface lenses. We further demonstrate multiwavelength color imaging with a high spatial resolution. Finally, optical imaging functionality with simultaneous color separation has been obtained by using multifunctional metasurfaces, which opens up new opportunities for the field of advanced imaging and display.

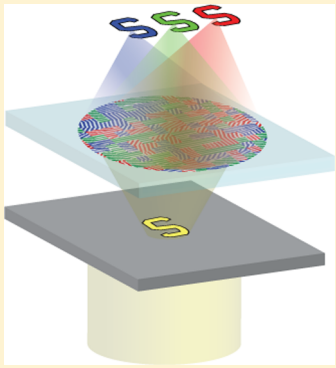

KEYWORDS: *Metasurfaces, multifunctional optics, phased array antenna, spatial multiplexing, geometric phase*

Metasurfaces have started to replace bulky optical components with ultrathin planar elements.[1−7] Metasurfaces are two-dimensional optical elements composed of a dense array of metallic or dielectric optical nanoantennas capable of manipulating light by imparting space-varying local amplitude and phase changes on incident electromagnetic waves.[7−12] Metasurfaces have been used to create optical elements that focus or redirect light,[13−17] control the state-of-polarization,[18,19] generate an amplified photonic spin Hall effect,[20,21] produce holograms,[22,23] concentrate nonlinearly generated light,[24] and even actively modulate the intensity.[25,26] Dielectric gradient metasurfaces, which avoid the optical losses typically associated with the use of metallic antennas by using low-loss dielectric nanostructures, have been investigated to achieve ultracompact beam manipulation and wavefront control[9,27] as well as high diffraction efficiencies in the visible and near-IR spectrum.[17,28] Moreover, dielectric metasurfaces based on geometric phase[1,2,9,13,29,30] can be easily patterned into a single layer of high index material.

Silicon-based gradient metasurfaces have been demonstrated by patterning an ultrathin Si film into a dense arrangement of nanobeams.[9] Because these metasurface-based optical elements are ultrathin and flat, they can be realized using commercially available fabrication facilities, making them easier to fabricate than multilevel diffractive optical elements. As a result, they could have a major impact on advanced imaging by reducing the size and complexity of imaging systems. Recently, metasurface lenses at visible wavelengths have been developed for imaging,[17,31] but their use has been limited to single wavelength applications chiefly due to the large degree of chromatic aberration in the lens design. Although various efforts have been made to avoid this problem,[32−34] achromatic imaging based on metasurfaces at visible wavelengths is still not available.

Here, we create a multifunctional metasurface lens (MML) by capitalizing on developments in interleaved phased array antenna technology[35−39] and Si-based gradient metasurfaces.[9] We show that, by interleaving multiple distinct optical elements, multifunctional wavefront shaping can be accomplished within a single shared aperture,[11,12] without reducing the numerical aperture of each subelement. Two MMLs constructed from Si nanobeam antennas[9,40,41] are realized as proof of this concept: an axial and lateral multifocus metasurface lens. Imaging systems using these MMLs are also implemented, demonstrating imaging at multiple wavelengths and simultaneous color separation using a single metasurface-based optical element.

Received: September 4, 2016
Revised: November 10, 2016
Published: November 18, 2016

DOI: 10.1021/acs.nanolett.6b03505
Nano Lett. 2016, 16, 7671−7676

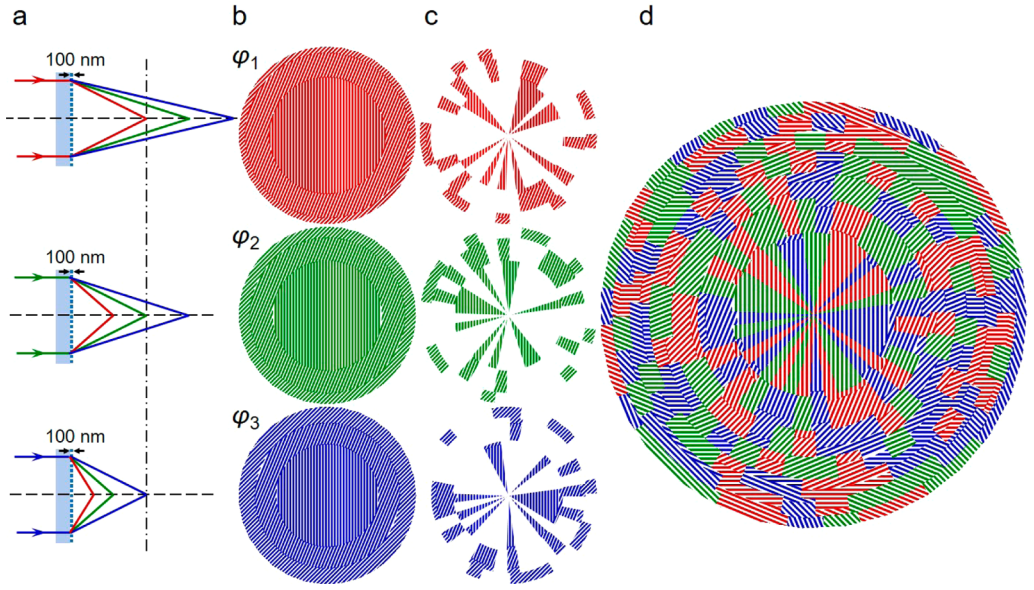

Figure 1. (a) Schematic of three MLs designed to focus light of different wavelength to the same focal plane. Each lens displays significant chromatic aberration. (b) Illustration of the nanopattern design of the MLs in panel a. (c) The three lenses in panel b are divided into a set of small subelements and complementary elements are chosen from each lens. (d) A composite, multifunctional metasurface lens created from the subelements from the original lenses. The composite lens offers multiwavelength focusing to a shared focal plane.

Figure 1 illustrates how we construct interleaved Si-based metasurfaces to achieve multiple functions within a shared surface region or aperture. We first demonstrate a transmissive axial MML that can focus three primary red, green, and blue (RGB) wavelengths (i.e., colors) to the same focal spot located at a well-defined focal plane behind the lenses, something that cannot be achieved with noninterleaved geometric phase metasurfaces. The axial MML is composed of three interleaved metasurface lenses (MLs) which respectively focus red, green, or blue to the same focal plane. The target phase profile φ_j of each sublens j is given by $\varphi_j(r) = \frac{2\pi}{\lambda_j}(f - \sqrt{r^2 + f^2})$, where f = 100 μm is the shared focal length for λ_j = 480, 550, and 620 nm, and r is the radial coordinate. The ray tracing scheme for RGB colors of each individual lens is depicted in Figure 1a; for example, the first lens focuses incident red light at the designed focal plane located 100 μm behind the lens. This single metasurface lens will also focus shorter wavelengths at a larger distance, resulting in separate foci for green and blue light incident on this MML. Note that the three lenses in Figure 1a share the same focal distance of 100 μm (vertical dashed line in Figure 1a) when illuminated by the three RGB colors.

The interleaved phase distribution is implemented using Si nanobeams[9] that can serve as half waveplates when placed into an array with a judiciously chosen spacing. The MML is constructed by patterning the surface with many such waveplates while spatially varying their orientation in order to control the local phase response to incident light. Circularly polarized light incident on the nanobeams is converted into light of the opposite helicity with a geometric phase φ_g given by $\varphi_g(x,y) = 2\sigma_\pm\theta(x,y)$, where $\sigma_\pm = \pm 1$ denotes the polarization helicity of the incident light and $\theta(x,y)$ is the in-plane orientation of the constituent waveplates. In this work, we created Si nanobeams with a thickness of 100 nm, a width of 120 nm, and a spacing of 80 nm by etching a 100 nm polycrystalline Si film on a glass substrate. The designed nanopatterns are shown in Figure 1b, where the colored stripes represent the nanobeams and the white areas represent the etched regions. The shown color of the stripes corresponds to the wavelength of the incident light that will be focused by the metasurface lens at the target focal plane. We approximate the smooth phase distributions of the ML by concentric rings each having discrete phase levels φ_g between 0 and 2π, linked to 8 discrete nanobeam orientations $\theta(x,y)$ between 0 and π.

To generate a MML we subsequently spatially multiplex the three phase profiles described above. First we divide each 100 μm^2 lens into segments with areas ~1 μm^2 by radially cutting across and along the concentric rings. This choice strikes a balance between achieving a smoothly varying phase profile and a high focusing efficiency as described in Supplementary Section 2. These segments are then distributed across the shared area of the MML with randomized tangential offsets, and allocating one-third of the area in each concentric ring to each of the three sublenses. This randomized distribution provides equal weight to each sublens and minimizes diffractive artifacts. The segments from the center region of each sublens are shown in Figure 1c. These segments fit together to form a single, multiwavelength lens that fills the entire surface area as shown in Figure 1d.

Figure 2 shows a scanning electron microscope (SEM) image of the fabricated MML comprised of Si nanobeam antennas with subwavelength spacing and space-varying orientations, fabricated by lithographic means.[9] When illuminated by a normally incident left circularly polarized (LCP) light beam, this three-element MML is capable of focusing the light into three focal points along the propagation axis. The intensity distribution of the light transmitted through the metasurface was measured using a confocal microscope setup.[9] Figure 2b shows the measured intensity distributions in the $x-z$ plane on the transmission side of the metasurface upon illumination with 480, 550, and 620 nm wavelength light, respectively. The intensity profiles show three focal spots for each single wavelength of illumination. All three colors are seen to focus to a shared focal plane at a distance of 100 μm behind the lens.

DOI: 10.1021/acs.nanolett.6b03505
Nano Lett. 2016, 16, 7671−7676

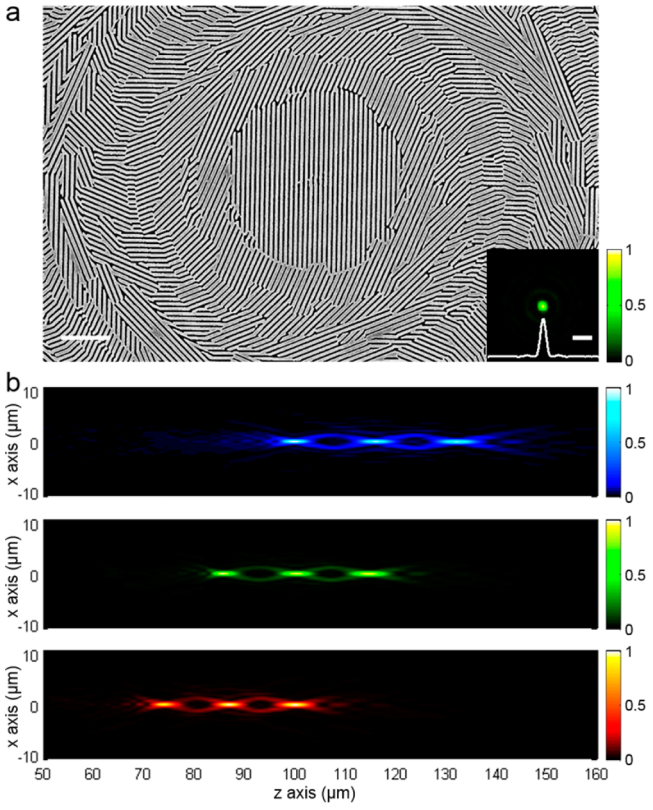

Figure 2. (a) SEM image of a fabricated axial MML. The inset shows a two-dimensional intensity profile in the focal plane 100 μm behind the MML at a wavelength of 550 nm. The intensity distribution through the focus is shown along the horizontal axis. The scale bars are 2 μm. (b) Measured intensity profiles on the transmission side of the axial MML along the $x-z$ plane upon illumination with light of 480, 550, and 620 nm in wavelength, respectively.

Therefore, a MML with multiple axial focal spots can generate a multiwavelength focal spot on the designed plane. Such a component can be used for multiwavelength imaging systems or to minimize chromatic aberrations in color imaging.

The focal spots generated by the MML are near diffraction-limited, with spot sizes with a full width half maximum of 683 nm at wavelength of 550 nm and equal to those obtained by a single, nonmultiplexed lens of the same diameter of 96 μm and numerical aperture (NA) of 0.43 (Figure S1). By utilizing our multiplexing scheme, the effective diameter of each sublens is equal to that of a single lens, and thus each sublens has the same numerical aperture as the single, full lens. Therefore, the multiplexed MML provides an enhanced NA compared to multifunctional optical elements in which the functional elements are spatially separated (see Figure S1). The achievement of multiple optical functionalities without compromising spatial resolution comes at the cost of a loss in peak intensity of the focused light. The randomized segmentation of the lenses generates an undesired speckle that removes intensity from the foci, which has been predicted to result in a peak intensity that scales as $1/N_c^2$, where N_c is the number of functions in the multiplexed lens[12] (Figure S1). In many imaging applications a high spatial resolution is more desirable than a high intensity, since the latter can be mitigated with improved illumination and detection optics. Also other methods of multiplexing could be explored to further increase the intensity.[12]

The principle of spatial multiplexing can be applied to realize a wide range of multifunctional metasurfaces. The optical elements that are incorporated in the metasurface can be chosen to meet the requirements for different applications. For applications where it is desirable to separate light of different wavelengths (colors), we designed a MML with multiple lateral focal spots for incident red, green and blue light. Figure 3a shows schematics of light rays focused and steered by individual

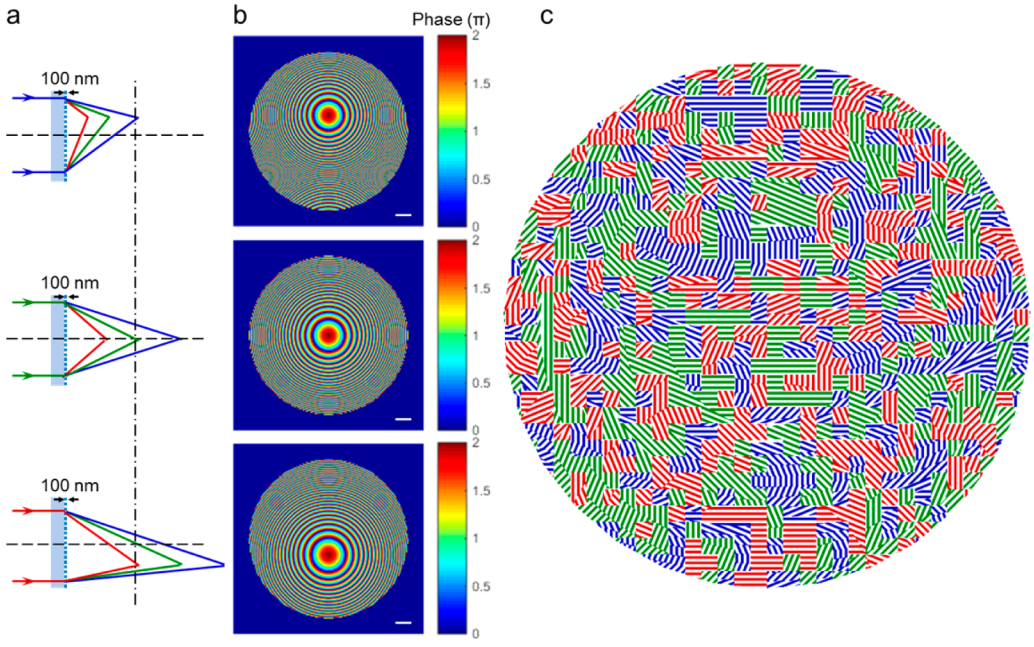

Figure 3. (a) Schematic of light rays focused and steered by individual laterally displaced MLs, with a focal length of 100 μm at wavelengths of 480, 550, and 620 nm, respectively. The focal spots are laterally separated for the three wavelengths. (b) Corresponding phase profiles of the metasurfaces. (c) Nanopattern design of an MML that incorporates the optical functions of the three MLs. The colored areas are segments taken from the lenses that focus blue, red, and green light to the same focal plane 100 μm away from the MML.

DOI: 10.1021/acs.nanolett.6b03505
Nano Lett. 2016, 16, 7671−7676

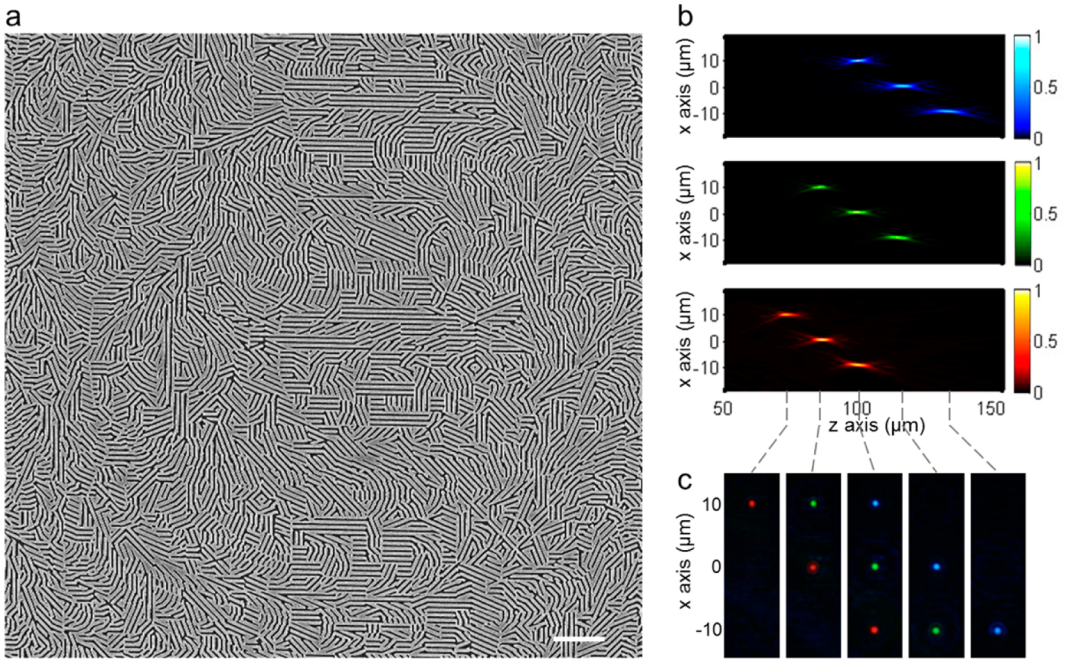

Figure 4. (a) Scanning electron microscope images of the fabricated color separating MML. The scale bar is 2 μm. (b) Measured intensity profile behind the MML in the $x-z$ plane upon illumination with 480, 550, and 620 nm wavelength, respectively. (c) Measured images at different distances on the z-axis. The connecting dashed lines indicate the corresponding image locations behind the MML.

MLs, with a shared focal length of 100 μm at wavelengths of 480, 550, and 620 nm, respectively. At the same time, the focal spots are laterally separated in the focal plane by 10 μm for the three wavelengths. Due to chromatic aberration, additional focal spots appear at additional distances when the optical elements are illuminated with multicolor light. The phase profiles for MLs that can focus and steer light at the same time are shown in Figure 3b. In order to realize the desired optical functionality, the phase profiles φ_j of the three individual MLs ($j = 1, 2, 3$) need to satisfy the relation $\varphi_j(r) = \frac{2\pi}{\lambda_j}(f - \sqrt{(x-d_j)^2 + y^2 + f^2})$ where $d_j = 10$, 0, and -10 μm, respectively, corresponding to the chosen lateral positions of the focal spots of different colors, and $f = 100$ μm is the focal length at $\lambda_j = 480$, 550, and 620 nm. The phase profiles can be recognized as lenses with displaced optical axes. These phase profiles are again implemented as gradient metasurfaces, and the three distinct optical elements are integrated into a single MML by using spatial multiplexing. Unlike the preceding case, the phase profile is no longer centrosymmetric, and consequently a different segmentation strategy is used. Here, the lens is divided into randomly placed 600×600 nm^2 segments arranged on a square lattice. Figure 3c shows the resulting nanopattern design that incorporates the optical functions of the three metasurface lenses. The stripes in the nanopattern represent Si nanobeams, and the colors indicate from which original sublens they were taken.

When illuminated by a monochromatic collimated LCP Gaussian beam, this MML (Figure 4a) is capable of focusing the light into three focal spots at different locations in both the lateral and axial direction. Figure 4b shows the measured intensity distributions in the $x-z$ plane on the transmission side of the metasurface upon illumination with 480, 550, and 620 nm wavelength light, respectively. The MML is seen to focus the three colors at the same focal plane ($z = 100$ μm) but steers light of different wavelengths to a different positions in the focal plane and thus afford spectral separation as designed. Figure 4c shows images recorded by a color CCD under simultaneous RGB illumination, representing the intensity distribution at different distances from the MML. At distances other than the designed focal length of 100 μm additional foci appear. For example, at a distance of 87 μm from the ML, green and red light is approximately focused by the sublenses designed for blue and green light, respectively.

The previous examples all involved normal-incidence, plane-wave illumination. In contrast, imaging of an extended object involves incident light covering a range of incident angles. In the following we experimentally demonstrate a multiwavelength imaging system using the MML design discussed above. A schematic of the imaging system using a MML is shown in Figure 5a. Figure 5b and c shows the imaging properties for the previously discussed color separating MML (Figures 3 and 4 and Figure S5b). Here, we use an object that has a clear area in the shape of the letter "S" with a width of 4 μm on an aluminum background. When illuminated by a supercontinuum white light source that is spectrally filtered to transmit red, green, and blue light, the object appears white (Figure 5b). After the light passes through the MML, RGB colors are steered to different lateral directions through different sublenses, respectively, but come into focus at the same image plane (Figure 5c). Indeed, laterally displaced red, green, and blue images of the letter "S" are formed on the shared image plane corresponding to the focal length of 100 μm (see Figure S7, Supplementary S8). Note that the MML can resolve the micrometer-sized target feature with similar image quality as the nonmultiplexed ML. Therefore, the MML carries out focusing and color separation at the same time, which could not have been achieved by using a single optical element.

In conclusion, the presented spatial interleaving approach for gradient metasurfaces enables the realization of multifunctional optical elements patterned within a single surface area. These multiplexed optical elements can achieve new optical

DOI: 10.1021/acs.nanolett.6b03505
Nano Lett. 2016, 16, 7671−7676

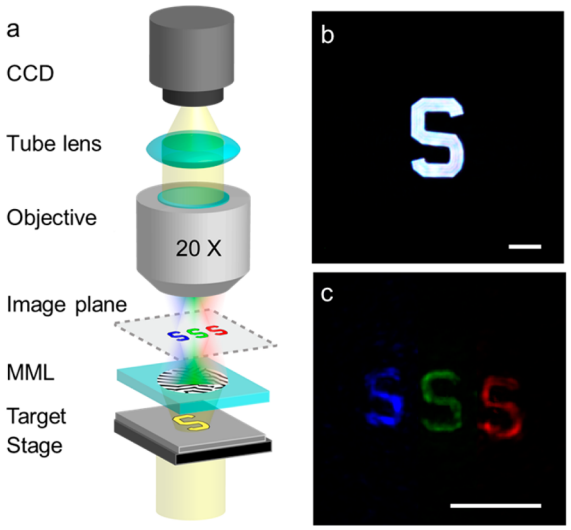

Figure 5. (a) Schematic of the optical microscope setup that uses the fabricated MML to image objects of interest. (b) Optical microscopy image of target shows the letter "S" on an aluminum background that appears white when illuminated with collimated lasers with RGB colors, and (c) image generated by the color separating MML, which separates different colors at different locations on the imaging plane. The scale bar is 10 μm.

functionalities that are unattainable by conventional optical components. The numerical aperture of the multifunctional lens is preserved when increasing the number of subelements N_c enabling multiple simultaneous optical functionalities that provide high spatial resolution. This design principle can be applied to other metasurfaces and across a wide range of the electromagnetic spectrum. MML make it possible to combine several of the necessary optical functions within an ultrathin planar optical element, which simplifies the form factor and complexity of imaging systems and offers new functionalities as compared to standard imaging systems. The demonstration of multifunctional metasurface lenses paves the way for future applications in advanced imaging and display technologies.

Methods. *Fabrication of Metasurface Lenses.* The metasurface lenses were generated in a single layer of nanopatterning. First, a 100 nm thick intrinsic poly-Si film was deposited onto a quartz substrate in a low-pressure chemical vapor deposition tool at 620 °C. Then, electron beam lithography using positive resist was employed to pattern the Si nanobeam locations and orientations, followed by standard reactive-ion etching (HBr/Cl_2) to transfer the nanopattern into the poly-Si layer.

Optical Characterization. 3D intensity distributions generated by the metasurface lenses (Figure 2b and Figure 4b) were measured using an optical microscope as shown in Figure 5a. For these measurements, metasurfaces are directly illuminated with a collimated laser beam with a beam width of 1 mm. The illumination source is a supercontinuum white light source that is wavelength-tunable from 400 to 2200 nm (NKT, SuperK Extreme). By using computer controlled spectral filters, it can serve as spectrally programmable laser with up to 16 simultaneous lines, making it possible to achieve simultaneous RGB laser illumination. A linear polarizer and a broadband quarter waveplate are utilized to generate a right circularly polarized (RCP) illumination beam. The intensity of the transmitted beam is recorded by a high-resolution CCD camera (Princeton Instruments, PIXIS 1024B).

In the imaging measurements (Figure 5b–c), a setup was used as schematically shown in Figure 5a. The target is placed on the microscope stage while the ML is mounted on an XYZ scanning stage with the patterned side facing the microscope objective. The real image generated by the MML is located at the focal plane of optical microscope. It is magnified and captured by the optical microscope and recorded by the high-resolution CCD camera. A circular polarizer is added before the CCD to filter out any transmitted RCP signal, which also removes the zero order transmitted beam.

■ ASSOCIATED CONTENT

Supporting Information

The Supporting Information is available free of charge on the ACS Publications website at DOI: 10.1021/acs.nanolett.6b03505.

Details on spatial multiplexing approach, schematics of the systems used for optical imaging, and additional experimental results that support the claims of the main text (PDF)

■ AUTHOR INFORMATION

Corresponding Author

*E-mail: brongersma@stanford.edu.

ORCID

Mark L. Brongersma: 0000-0003-1777-8970

Notes

The authors declare no competing financial interest.

■ ACKNOWLEDGMENTS

We acknowledge funding support from the United States-Israel Binational Science Foundation (BSF), the Global Climate and Energy Project, and a Multi-University Research Initiative funded by the U.S. Airforce Office for Science Research Grant No. FA9550-14-1-0389. A.L.H. acknowledges support from an Air Force Office of Scientific Research, National Defense Science and Engineering Graduate (NDSEG) Fellowship, 32 CFR 168a. We are grateful to James Conway for his assistance in nanopatterning. We also thank Isaac Kauvar for helpful discussions.

■ REFERENCES

(1) Bomzon, Z.; Kleiner, V.; Hasman, E. Pancharatnam-Berry phase in space-variant polarization-state manipulations with subwavelength gratings. *Opt. Lett.* **2001**, *26*, 1424–1426.

(2) Bomzon, Z.; Biener, G.; Kleiner, V.; Hasman, E. Space-variant Pancharatnam–Berry phase optical elements with computer-generated subwavelength gratings. *Opt. Lett.* **2002**, *27*, 1141–1143.

(3) Lalanne, P.; Astilean, S.; Chavel, P.; Cambril, E.; Launois, H. Blazed binary subwavelength gratings with efficiencies larger than those of conventional échelette gratings. *Opt. Lett.* **1998**, *23*, 1081–1083.

(4) Lalanne, P.; Astilean, S.; Chavel, P.; Cambril, E.; Launois, H. Design and fabrication of blazed binary diffractive elements with sampling periods smaller than the structural cutoff. *J. Opt. Soc. Am. A* **1999**, *16*, 1143–1156.

(5) Verslegers, L.; Catrysse, P. B.; Yu, Z. F.; White, J. S.; Barnard, E. S.; Brongersma, M. L.; Fan, S. H. Planar Lenses Based on Nanoscale Slit Arrays in a Metallic Film. *Nano Lett.* **2009**, *9*, 235–238.

(6) Ni, X. J.; Emani, N. K.; Kildishev, A. V.; Boltasseva, A.; Shalaev, V. M. Broadband Light Bending with Plasmonic Nanoantennas. *Science* **2012**, *335*, 427.

DOI: 10.1021/acs.nanolett.6b03505
Nano Lett. 2016, 16, 7671–7676

(7) Pors, A.; Albrektsen, O.; Radko, I. P.; Bozhevolnyi, S. I. Gap plasmon-based metasurfaces for total control of reflected light. *Sci. Rep.* **2013**, *3*, 2155.
(8) Yu, N. F.; Genevet, P.; Kats, M. A.; Aieta, F.; Tetienne, J. P.; Capasso, F.; Gaburro, Z. Light Propagation with Phase Discontinuities: Generalized Laws of Reflection and Refraction. *Science* **2011**, *334*, 333−337.
(9) Lin, D. M.; Fan, P. Y.; Hasman, E.; Brongersma, M. L. Dielectric gradient metasurface optical elements. *Science* **2014**, *345*, 298−302.
(10) Chong, K. E.; Staude, I.; James, A.; Dominguez, J.; Liu, S.; Campione, S.; Subramania, G. S.; Luk, T. S.; Decker, M.; Neshev, D. N.; et al. Polarization-Independent Silicon Metadevices for Efficient Optical Wavefront Control. *Nano Lett.* **2015**, *15*, 5369−5374.
(11) Veksler, D.; Maguid, E.; Shitrit, N.; Ozeri, D.; Kleiner, V.; Hasman, E. Multiple Wavefront Shaping by Metasurface Based on Mixed Random Antenna Groups. *ACS Photonics* **2015**, *2*, 661−667.
(12) Maguid, E.; Yulevich, I.; Veksler, D.; Kleiner, V.; Brongersma, M. L.; Hasman, E. Photonic spin-controlled multifunctional shared-aperture antenna array. *Science* **2016**, *352*, 1202−1206.
(13) Hasman, E.; Kleiner, V.; Biener, G.; Niv, A. Polarization dependent focusing lens by use of quantized Pancharatnam-Berry phase diffractive optics. *Appl. Phys. Lett.* **2003**, *82*, 328−330.
(14) Fattal, D.; Li, J. J.; Peng, Z.; Fiorentino, M.; Beausoleil, R. G. Flat dielectric grating reflectors with focusing abilities. *Nat. Photonics* **2010**, *4*, 466−470.
(15) Ishii, S.; Kildishev, A. V.; Shalaev, V. M.; Chen, K.-P.; Drachev, V. P. Metal nanoslit lenses with polarization-selective design. *Opt. Lett.* **2011**, *36*, 451−3.
(16) Arbabi, A.; Horie, Y.; Ball, A. J.; Bagheri, M.; Faraon, A. Subwavelength-thick lenses with high numerical apertures and large efficiency based on high-contrast transmitarrays. *Nat. Commun.* **2015**, *6*, 7069.
(17) Khorasaninejad, M.; Chen, W. T.; Devlin, R. C.; Oh, J.; Zhu, A. Y.; Capasso, F. Metalenses at visible wavelengths: Diffraction-limited focusing and subwavelength resolution imaging. *Science* **2016**, *352*, 1190−1194.
(18) Bomzon, Z.; Biener, G.; Kleiner, V.; Hasman, E. Radially and azimuthally polarized beams generated by space-variant dielectric subwavelength gratings. *Opt. Lett.* **2002**, *27*, 285−287.
(19) Zeng, J.; Gao, J.; Luk, T. S.; Litchinitser, N. M.; Yang, X. Structuring Light by Concentric-Ring Patterned Magnetic Metamaterial Cavities. *Nano Lett.* **2015**, *15*, 5363−5368.
(20) Shitrit, N.; Bretner, I.; Gorodetski, Y.; Kleiner, V.; Hasman, E. Optical Spin Hall Effects in Plasmonic Chains. *Nano Lett.* **2011**, *11*, 2038−2042.
(21) Yin, X.; Ye, Z.; Rho, J.; Wang, Y.; Zhang, X. Photonic Spin Hall Effect at Metasurfaces. *Science* **2013**, *339*, 1405−1407.
(22) Ni, X.; Kildishev, A. V.; Shalaev, V. M. Metasurface holograms for visible light. *Nat. Commun.* **2013**, *4*, 2807.
(23) Zheng, G.; Mühlenbernd, H.; Kenney, M.; Li, G.; Zentgraf, T.; Zhang, S. Metasurface holograms reaching 80% efficiency. *Nat. Nanotechnol.* **2015**, *10*, 308−312.
(24) Segal, N.; Keren-zur, S.; Hendler, N.; Ellenbogen, T. Controlling light with metamaterial-based nonlinear photonic crystals. *Nat. Photonics* **2015**, *9*, 180−184.
(25) Sautter, J.; Staude, I.; Decker, M.; Rusak, E.; Neshev, D. N.; Brener, I.; Kivshar, Y. S. Active Tuning of All-Dielectric Metasurfaces. *ACS Nano* **2015**, *9*, 4308−4315.
(26) Wang, Q.; Rogers, E. T. F.; Gholipour, B.; Wang, C.-M.; Yuan, G.; Teng, J.; Zheludev, N. I. Optically reconfigurable metasurfaces and photonic devices based on phase change materials. *Nat. Photonics* **2015**, *10*, 60−65.
(27) Shalaev, M. I.; Sun, J.; Tsukernik, A.; Pandey, A.; Nikolskiy, K.; Litchinitser, N. M. High-Efficiency All-Dielectric Metasurfaces for Ultracompact Beam Manipulation in Transmission Mode. *Nano Lett.* **2015**, *15*, 6261−6266.
(28) Arbabi, A.; Horie, Y.; Bagheri, M.; Faraon, A. Dielectric metasurfaces for complete control of phase and polarization with subwavelength spatial resolution and high transmission. *Nat. Nanotechnol.* **2015**, *10*, 937−943.
(29) Biener, G.; Niv, A.; Kleiner, V.; Hasman, E. Formation of helical beams by use of Pancharatnam-Berry phase optical elements. *Opt. Lett.* **2002**, *27*, 1875−1877.
(30) Niv, A.; Biener, G.; Kleiner, V.; Hasman, E. Manipulation of the Pancharatnam phase in vectorial vortices. *Opt. Express* **2006**, *14*, 4208−4220.
(31) Chen, X. Z.; Huang, L. L.; Muhlenbernd, H.; Li, G. X.; Bai, B. F.; Tan, Q. F.; Jin, G. F.; Qiu, C. W.; Zhang, S.; Zentgraf, T. Dual-polarity plasmonic metalens for visible light. *Nat. Commun.* **2012**, *3*, 1198.
(32) Aieta, F.; Kats, M. A.; Genevet, P.; Capasso, F. Multiwavelength achromatic metasurfaces by dispersive phase compensation. *Science* **2015**, *347*, 1342−1345.
(33) Khorasaninejad, M.; Aieta, F.; Kanhaiya, P.; Kats, M. A.; Genevet, P.; Rousso, D.; Capasso, F. Achromatic Metasurface Lens at Telecommunication Wavelengths. *Nano Lett.* **2015**, *15*, 5358−5362.
(34) Arbabi, E.; Arbabi, A.; Kamali, S. M.; Horie, Y.; Faraon, A. Multiwavelength polarization-insensitive lenses based on dielectric metasurfaces with meta-molecules. *Optica* **2016**, *3*, 628−633.
(35) Pozar, D. M.; Targonski, S. D. A shared-aperture dual-band dual-polarized microstrip array. *IEEE Trans. Antennas Propag.* **2001**, *49*, 150−157.
(36) Haupt, R. L. Interleaved Thinned Linear Arrays. *IEEE Trans. Antennas Propag.* **2005**, *53*, 2858−2864.
(37) Sayeed, A. M.; Member, S.; Raghavan, V. Maximizing MIMO Capacity in Sparse Multipath With Reconfigurable Antenna Arrays. *IEEE J. Sel. Top. Signal Process* **2007**, *1*, 156−166.
(38) Lager, I. E.; Trampuz, C.; Simeoni, M.; Ligthart, L. P. Interleaved Array Antennas for FMCW Radar Applications. *IEEE Trans. Antennas Propag.* **2009**, *57*, 2486−2490.
(39) LeCompte, M.; Shi, S. Y.; Prather, D. W. Interleaved diffractive optical element design. *Proc. SPIE* **2001**, *4436*, 115−122.
(40) Cao, L. Y.; Fan, P. Y.; Barnard, E. S.; Brown, A. M.; Brongersma, M. L. Tuning the Color of Silicon Nanostructures. *Nano Lett.* **2010**, *10*, 2649−2654.
(41) Cao, L. Y.; White, J. S.; Park, J. S.; Schuller, J. A.; Clemens, B. M.; Brongersma, M. L. Engineering light absorption in semiconductor nanowire devices. *Nat. Mater.* **2009**, *8*, 643−647.

DOI: 10.1021/acs.nanolett.6b03505
Nano Lett. 2016, 16, 7671−7676